SHORT REPORT

COM-1 and Hongcheon: New monazite reference materials for the microspot analysis of oxygen isotopic composition

Jeongmin Kim[1], Changkun Park[2], Keewook Yi[1], Shinae Lee[1], Sook Ju Kim[1], Min-Ji Jung[1,3] and Albert Chang-sik Cheong[1,3*]

Abstract

Background: Monazite, a moderately common light rare earth element (LREE) and thorium phosphate mineral, has chemical, age, and isotopic characteristics that are useful in the investigation of the origin and evolution of crustal melts and fluid-rock interactions. Multiple stages of growth and partial recrystallization commonly observed in monazite inevitably require microspot chemical and isotopic analyses, for which well-characterized reference materials are essential to correct instrumental biases. In this study, we introduce new monazite reference materials COM-1 and Hongcheon for the use in the microspot analysis of oxygen isotopic composition.

Findings: COM-1 and Hongcheon were derived from a late Mesoproterozoic (~ 1080 Ma) pegmatite dyke in Colorado, USA, and a Late Triassic (~ 230 Ma) carbonatite-hosted REE ore in central Korea, respectively. The COM-1 monazite has much higher levels of Th (8.77 ± 0.56 wt.%), Si (0.82 ± 0.07 wt.%) and lower REE contents (total REE $= 49.5 \pm 1.2$ wt.%) than does the Hongcheon monazite (Th, 0.23 ± 0.11 wt.%; Si, < 0.1 wt.%; total REE, 59.9 ± 0.7 wt.%). Their oxygen isotopic compositions ($\delta^{18}O_{VSMOW}$) were determined by gas-source mass spectrometry with laser fluorination (COM-1, 6.67 ± 0.08‰; Hongcheon-1, 6.60 ± 0.02‰; Hongcheon-2, 6.08 ± 0.07‰). Oxygen isotope measurements performed by a Cameca IMS1300-HR^3 ion probe showed a strong linear dependence ($R^2 = 0.99$) of the instrumental mass fractionation on the total REE contents.

Conclusions: We characterized chemical and oxygen isotopic compositions of COM-1 and Hongcheon monazites. Their internal homogeneity in oxygen isotopic composition and chemical difference provide an efficient tool for calibrating instrumental mass fractionation occurring during secondary ion mass spectrometry analyses.

Keywords: Monazite, Reference material, COM-1, Hongcheon, Oxygen isotopes, Instrumental mass fractionation

Introduction

Geological and environmental samples are commonly composed of chemically or isotopically heterogeneous domains that may have their own genetic significance. The high sensitivity and spatial resolution of modern microbeam techniques, typically on micrometer or submicrometer scale, allow researchers to analyze individual micro-domains with no significant loss of analytical precision. The integration of multifaceted data from single microspots has opened new avenues in geochemical research. For example, the cool early Earth hypothesis was suggested by multiple lines of evidence from a single Hadean zircon (Valley, 2005). Microanalytical data combined with textural and petrographic observations revealed that mineral phases in igneous rocks are commonly not in isotopic equilibrium with their groundmass, reflecting progressive changes in magma composition (Davidson et al., 2007).

*Correspondence: ccs@kbsi.re.kr

[1] Korea Basic Science Institute, Cheongju 28119, Republic of Korea
Full list of author information is available at the end of the article

Kim *et al. Journal of Analytical Science and Technology*　　(2022) 13:34

Page 2 of 8

Chemical and isotopic data obtained from microbeam analyses should be corrected and calibrated due to instrumental biases; this goal is typically achieved using matrix-matched reference materials (RMs) to check data accuracy and, more importantly, to calculate inter-elemental isotopic ratios or instrumental mass fractionation (IMF) factors. In the latter case, the reference value should be measured and evaluated with great care because it directly affects the results for unknown samples. This is particularly true in the microspot measurement of the isotopic composition of oxygen, Earth's most abundant element.

Oxygen has three stable isotopes: ^{16}O ($\sim 99.76\%$), ^{17}O ($\sim 0.04\%$), and ^{18}O ($\sim 0.2\%$) (Meija et al., 2016). By convention, oxygen isotopic ratios are expressed using delta notation, relative to standard mean oceanic water (SMOW; $^{18}O/^{16}O = 0.0020052$; Baertschi, 1976), as follows:

$$\delta^{18}O_{SMOW} = \left[\left(^{18}O/^{16}O\right)_{sample} \middle/ \left(^{18}O/^{16}O\right)_{SMOW} \right] - 1$$

For most terrestrial fractionation processes, $\delta^{17}O$ correlates closely with $\delta^{18}O$ ($\delta^{17}O = \sim 0.52 \times \delta^{18}O$; Hoefs, 2018). Oxygen isotopic fractionation is associated chiefly with low-temperature surface processes because the log-transformed fractionation factor and temperature have an inverse quadratic relationship (Hoefs, 2018). ^{18}O and ^{17}O are concentrated on the surface because ^{16}O, the lighter isotope is released preferentially during weathering. Meteoric water is isotopically light as a result of Rayleigh distillation upon vapor transport and precipitation. Magma inherits the oxygen isotopic signatures of its sources or assimilants because isotopic fractionations among melts and minerals are relatively small at magmatic temperatures, typically less than 2‰. As documented in abundant literatures (*e.g.,* Faure and Mensing, 2005; Sharp, 2017; Hoefs, 2018), oxygen isotopes have become an essential tool for a wide range of geochemical and cosmochemical applications. The most precise method for oxygen isotope measurement in minerals is gas-source mass spectrometry with laser fluorination, a technique developed in the 1990s (Sharp, 1990). This bulk analysis provides a basis for the calibration of microspot data currently obtained by secondary ion mass spectrometry (SIMS).

Monazite, a light rare earth element (LREE) and thorium phosphate mineral commonly occurring in clastic sedimentary rocks, low- to medium-pressure metamorphic rocks, peraluminous granites, and hydrothermal ore deposits, is more likely to be affected by fluids and melts than silicate minerals and thus frequently found as a complexly zoned mineral (Foster et al., 2002; Catlos, 2013). Microspot oxygen isotope data obtained from individual zones, particularly when combined with geochronological and petrographic information, provide an excellent opportunity for the investigation of interactions between the hydrosphere and lithosphere. SIMS has been used for the analysis of oxygen isotopes in monazite and other phosphate minerals since the mid-2000s (Ayers et al., 2006; Breecker and Sharp, 2007); however, no consensus on IMF-related calibration has been reached (Rubatto et al., 2014; Didier et al., 2017) and the RMs required for monazite oxygen isotope analysis with SIMS remain insufficient. The matrix effect resulting from the common substitutions of huttonite ($ThSiO_4$) and cheralite [$CaTh(PO_4)_2$] into the monazite structure is non-negligible. Here, we present high-resolution SIMS and laser fluorination oxygen isotope data for new monazite RMs COM-1 and Hongcheon, along with chemical data obtained by an electron probe microanalyzer (EPMA) and laser ablation inductively coupled plasma mass spectrometry (ICP-MS).

Materials

The COM-1 monazite is a translucent pale-brown crystal obtained from a pegmatite dyke in Colorado, USA (Fig. 1), purchased by the Korea Basic Science Institute (KBSI) from eBay in 2014. No further information about the nature of its host rock is available. Kim et al. (2015) reported a weighted mean $^{206}Pb/^{238}U$ age of 1078.9 ± 5.0 Ma for this monazite, obtained using a sensitive high-resolution ion microprobe (SHRIMP IIe/MC) installed at the KBSI. This age is consistent with the SHRIMP $^{208}Pb/^{232}Th$ and laser ablation multi-collector ICP-MS $^{206}Pb/^{238}U$ ages also measured at the KBSI (1087.2 ± 8.4 and 1076.6 ± 9.4 Ma, respectively).

Hongcheon monazites were collected by Kim et al. (2016) from a Late Triassic carbonatite-hosted REE ore in central Korea (Fig. 1). The host rocks of Hongcheon-1 (sample 304-5A) and Hongcheon-2 (sample K12-A) were taken from an outcrop in the southern ore body ($37°51'41.8''$ N, $128°00'56.2''$ E) and a 76-m-deep core drilled into the central ore body, respectively. The former was a massive, medium- to coarse-grained pinkish carbonatite with interstitial patches of quartz aggregates and few magnetite grains. The latter was a massive, fine-grained pale-gray carbonatite with variable amounts of disseminated magnetite. Monazite grains separated from these samples yielded a SHRIMP $^{208}Pb/^{232}Th$ age of 232.9 ± 1.6 Ma (Kim et al., 2016). Their REE contents are relatively high (total REE oxide > 66 wt.%) and vary narrowly, irrespective of the textural occurrence. Thorium contents in Hongcheon monazites are relatively low (average = ~ 0.25 wt.%), and Th/U ratios are unusually high (average = ~ 2200). These chemical properties were confirmed in this study.

Kim *et al. Journal of Analytical Science and Technology*   (2022) 13:34
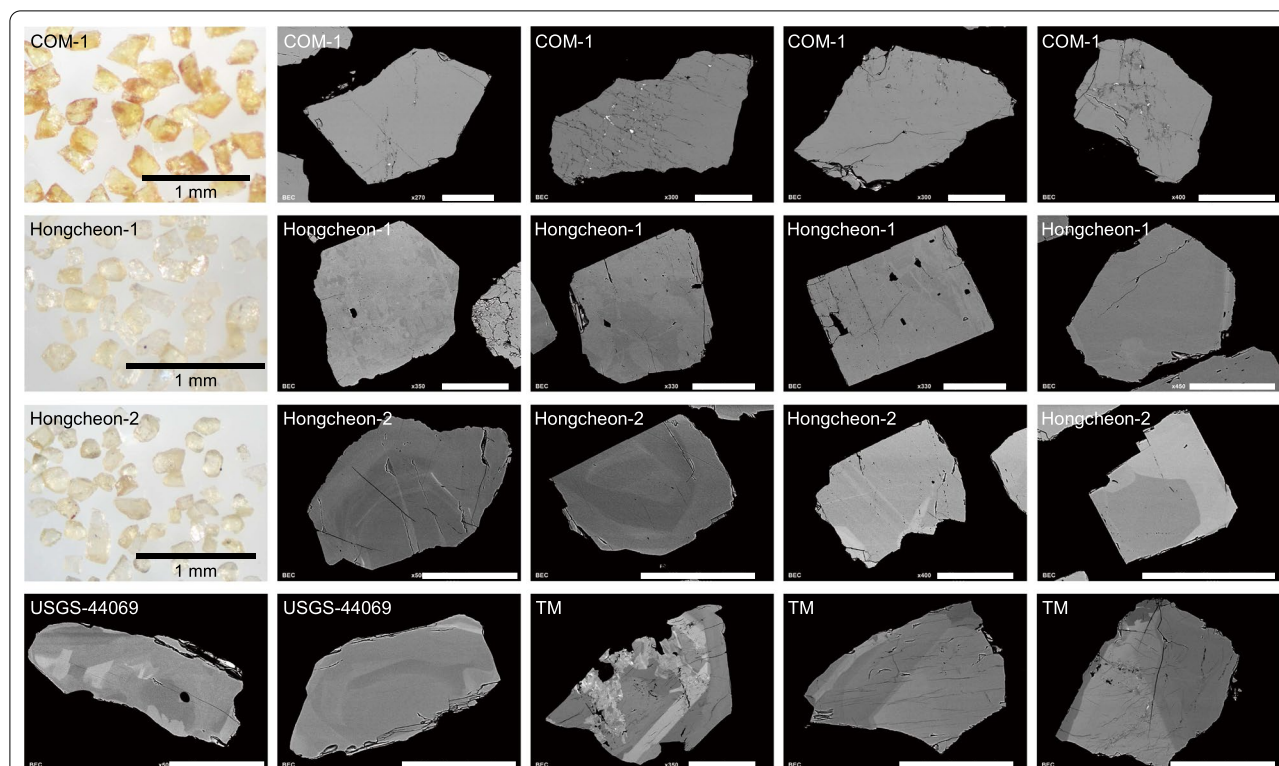
Page 3 of 8

Fig. 1 Sample photographs and representative backscattered electron images of the monazite reference materials. Scale bars in backscattered electron images are 100 μm

USGS-44069 and TM monazites were also analyzed in this study to ensure data accuracy. USGS-44069 originates from an amphibolite to granulite facies metasedimentary unit (the Wissahickon Formation) of the Wilmington Complex, Delaware, USA; it has a well-constrained thermal ionization mass spectrometric U/Pb age of 424.9 ± 0.4 Ma (Aleinikoff et al., 2006), which was interpreted to represent a metamorphic overprint. The grains are < 200 μm in diameter and honey-yellow in color. This monazite contains negligible huttonite substitution and variable amounts of cheralite, with a relatively low Th content (~ 2 wt.%) (Rubatto et al., 2014). The TM monazite is from the Thompson Nickel Mine, central Manitoba, Canada, and has been used as a U/Pb standard, with an age of 1766 Ma (Williams et al., 1996). The TM crystals are relatively large (several 100 s of microns in diameter) and yellow to orange in color, with a particularly high Th content of > 10 wt.% (Rubatto et al., 2014).

Methods

Monazite grains were embedded in epoxy and polished to expose a pristine surface. Backscattered electron (BSE) images of the grains were examined using a scanning electron microscope (JSM-6610LV; JEOL) at the KBSI. Chemical compositions of the monazites were determined at the Center for Research Facilities, Gyeongsang National University using an EPMA (JXA-8530F PLUS; JEOL) equipped with five wavelength-dispersive X-ray spectrometers. The acceleration voltage was set to 15 kV, and the beam current was set to 20 nA. The counting times for peaks were 10–30 s.

Monazites were also analyzed using a 343-nm femtosecond laser ablation microprobe (J200 LA; Applied Spectra Inc.) coupled with an iCapQ (Thermo Fisher Scientific) quadrupole ICP-MS at the Core Research Facilities of Pusan National University. The instrumental parameters for laser ablation and ICP-MS, basically the same as those in Cheong et al. (2019), were optimized to provide the highest sensitivity whilst maintaining the ratio of ThO^+/Th^+ below 0.005. External standardization was performed relative to NIST SRM 610–612 glasses (Jochum et al., 2011), and the internal standard was the Ce content measured by EPMA.

The bulk measurement of oxygen isotopes in the monazite grains was conducted using a dual-inlet gas-source mass spectrometer (MAT 253 Plus; Thermo Fisher Scientific) at the Korea Polar Research Institute (KOPRI). Several milligrams of monazite grains, ~ 100 μm in diameter, were selected carefully under microscopy to avoid any inclusion or coexisting mineral. At least three aliquots of

KOPRI in-house standard obsidian ($\delta^{18}O_{VSMOW} = 8.40‰$) were loaded into the reaction chamber with the monazite grains and analyzed before and after the monazite analyses to check the accuracy and external reproducibility of the oxygen isotope data. The reaction chamber containing obsidian and monazite grains was heated to 150 ℃ overnight in a vacuum to remove moisture adsorbed onto the sample surfaces. To remove any possible remaining moisture, a small amount of BrF_5 gas was introduced into the reaction chamber for 1 h, and the chamber was evacuated before the initiation of analysis. After prefluorination, ~110 mbar BrF_5 was introduced into the chamber and the sample was heated by gradually increasing the power of CO_2 laser to 15 W (60% of the maximum power). All gaseous species released from the samples were expanded to the first cryogenic trap and condensable gases at liquid nitrogen temperature (-196 ℃) were removed. Non-condensable F_2 gas was converted into bromine (Br_2) through the KBr getter, and the Br_2 was trapped in the second cryogenic trap. Finally, the purified O_2 gas was collected in a cryogenic trap containing a pellet of 13X molecular sieve (MS13X) for 15 min and released to the mass spectrometer at room temperature. This analytical procedure is described in greater detail elsewhere (Kim et al., 2019). A laboratory working standard O_2 gas ($\delta^{18}O_{VSMOW} = -9.62‰$) was calibrated by measuring oxygen isotopes of Vienna Standard Mean Ocean Water (VSMOW, $\delta^{18}O_{VSMOW} = 0‰$ per definition) and Standard Light Antarctica Precipitation (SLAP) with the same purification line (Kim et al., 2020). Although two-point normalization (VSMOW–SLAP) is recommended to correct inter-laboratory biases, we report $\delta^{18}O$ values relative to VSMOW to enable comparison of the values with data reported in the literature as $\delta^{18}O_{VSMOW}$. The precision of $\delta^{18}O$ measurement at KOPRI is typically < 0.15‰ [1 standard deviation (SD); Kim et al., 2020]. Some COM-1 monazite grains were sputtered and ejected from the sample holder during laser heating, resulting in a low O_2 gas yield and low $\delta^{18}O$ values (Additional file 1: Table S1). Previous studies have also addressed such issue related to laser fluorination of phosphate and particularly monazite (Breecker and Sharp, 2007; Rubatto et al., 2014). More experiments are needed to find optimum conditions of BrF_5 pressure and laser power to prevent violent reaction and to obtain high O_2 yield.

Monazite oxygen isotopes were also measured using a Cameca IMS1300-HR[3] large-geometry SIMS at the KBSI. The epoxy mount was Au-coated at a thickness of 20 nm for SIMS analysis. The analytical conditions are summarized in Additional file 2: Table S2. A focused Cs^+ primary ion beam (Gaussian mode) was accelerated at 10 kV, with an ion current of ~3.0 nA and a spot diameter of ~15 μm. Secondary ions were accelerated by -10 kV on the sample surface and transferred to field aperture. To maximize secondary ion transmission, the transfer lens optics were set to a magnification of ~200. The secondary ion beam was automatically centered on the field aperture and entrance slit/contrast aperture prior to each analysis. Charge buildup on the sample surface was compensated using a normal incidence electron gun. The contrast aperture, entrance slit, field aperture, and energy slit were set to 400 μm diameter, ~70.3 μm width, 3000×3000 μm², and 50 eV width at the low-energy peak, respectively. $^{16}O^-$ and $^{18}O^-$ ions were detected simultaneously using two Faraday cups with 10^{10} and 10^{11} Ω pre-amplifiers, respectively. A 500-μm exit slit with a mass-resolving power of ~2000, defined as M/ΔM at 50% peak height, was used for both detectors. Under these conditions, $^{16}O^-$ and $^{18}O^-$ count rates were typically ~3×10^9 cps and ~6×10^6 cps, respectively. The internal precision of $^{18}O/^{16}O$ measurement was ~0.2‰ (20 cycles, 2 standard errors).

Results and discussion
BSE texture and chemical composition
The BSE images (Fig. 1) showed no zoning in most COM-1 crystals, although some grains had linear patches of alteration along a network of microfractures. These grains contained inclusions of thorite, calcite, and biotite, mainly along the alteration zone. Hongcheon-1 crystals exhibited euhedral to subhedral external shapes. Some grains consisted of mosaics of patches, with weak contrast in BSE brightness. Inclusions of apatite, strontianite, dolomite, and Fe oxides were found in Hongcheon-1 monazites. Hongcheon-2 crystals also exhibited euhedral to subhedral external shapes. These grains showed BSE zoning with combinations of banded and patch patterns, which may have correlated with Th content (Möller et al., 2003; Rubatto et al., 2014). Inclusions were rare in Hongcheon-2 grains. As reported by Rubatto et al. (2014), USGS-44069 and TM monazites exhibited polygonal and oscillatory BSE zoning. Microfracture networks and alteration zones were commonly observed in TM crystals.
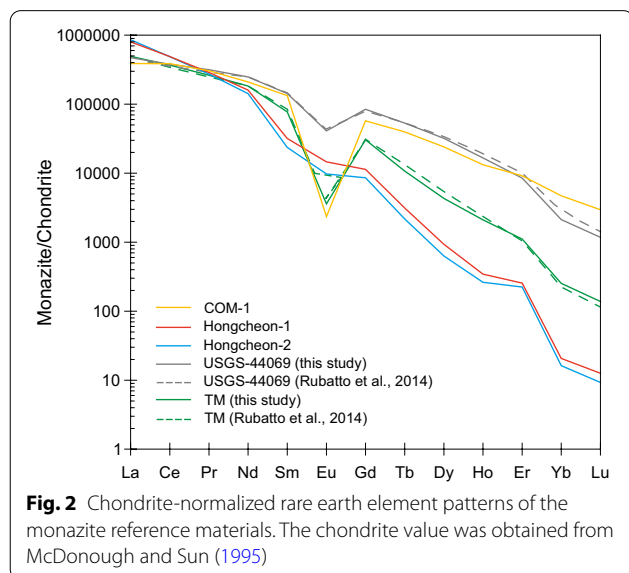
The chemical compositions of monazites analyzed by EPMA and laser ablation ICP-MS are listed in Additional file 3: Table S3 and Additional file 4: Table S4, respectively, and summarized in Table 1. Based on the ICP-MS data, COM-1 monazites had an average total REE content of 49.5 ± 1.2 wt.% (1 SD unless otherwise noted). The grains showed slightly positive Ce and distinctly negative Eu anomalies (Ce/Ce$^* = 1.13 \pm 0.05$; Eu/Eu$^* = 0.027 \pm 0.002$) in the chondrite-normalized (McDonough and Sun, 1995) diagram, with relatively low La/Yb ratios [(La/Yb)$_{normalized} = 84 \pm 11$; Fig. 2]. Thorium

Kim *et al. Journal of Analytical Science and Technology*   (2022) 13:34

Page 5 of 8

Table 1 Summary of monazite reference material compositions

	COM-1		Hongcheon-1		Hongcheon-2		USGS-44069		TM	
	Average	SD	Average	SD	Average	SD	Average	SD	Average	SD
EPMA data (in wt.%)										
SiO_2	1.75	0.15	b.d.l.		b.d.l.		0.09	0.06	1.36	0.43
CaO	0.80	0.07	0.06	0.03	0.07	0.03	0.77	0.16	1.59	0.26
P_2O_5	28.14	0.59	31.27	0.55	31.28	0.64	31.06	0.69	28.52	0.96
ThO_2	9.97	0.63	0.29	0.12	0.23	0.12	2.68	0.51	11.22	1.56
Laser ablation ICP-MS data (in ppm)										
Sr	43	48	2621	1411	2025	855	49	13	92	61
Y	8003	793	316	162	251	124	20,001	2903	2516	1067
La	92,007	4678	190,112	7619	204,141	6424	112,386	9276	117,092	4161
Ce*	236,997	3471	300,642	2143	299,541	2863	232,399	6615	225,543	9634
Pr	28,301	2303	26,713	1577	25,385	1275	29,371	2854	24,364	1135
Nd	95,954	4318	73,100	5891	64,889	3697	113,330	5557	83,776	3952
Sm	19,714	1153	4720	794	3506	463	21,131	2072	11,425	1014
Eu	132	11	822	170	549	114	2315	434	202	36
Gd	11,395	681	2261	354	1707	236	16,830	2211	6082	510
Tb	1432	118	113	29	78	17	1924	220	388	53
Dy	5918	376	230	89	155	54	7877	1070	1059	231
Ho	723	51	19	8	14	6	908	150	115	40
Er	1467	101	41	11	36	9	1358	232	178	73
Tm	157	17	0.9	0.5	0.8	0.5	95	23	10	6
Yb	757	120	3.3	1.5	2.6	1.3	342	104	41	26
Lu	73	16	0.3	0.2	0.2	0.1	29	9	3.4	2.2
U	2046	174	2.3	1.4	2.9	3.3	3764	991	1738	560
Pb	4914	384	35	12	25	16	795	157	8258	1255

b.d.l.: below detection limit

*EPMA data, internal standard

Fig. 2 Chondrite-normalized rare earth element patterns of the monazite reference materials. The chondrite value was obtained from McDonough and Sun (1995)

(8.77 ± 0.56 wt.%) and Si (0.82 ± 0.07 wt.%) contents (EPMA data) were relatively high. EPMA data-based mole fractions of huttonite and cheralite were determined to be 0.070 ± 0.006 and 0.100 ± 0.011, respectively.

As Kim et al. (2016) reported, Hongcheon monazites had small variations in total REE contents (59.9 ± 0.7 wt.%, ICP–MS data) and showed heavy REE-depleted chondrite-normalized patterns [average (La/Yb)$_{normalized}$ > 50,000], with no Ce and small Eu anomalies (Ce/Ce* = 1.02 ± 0.02; Eu/Eu* = 0.72 ± 0.07; Fig. 2). Relative to COM-1, they were strongly enriched in Sr (0.23 ± 0.12 wt.%) but depleted in Th (0.23 ± 0.11 wt.%, EPMA data) and U (<5 ppm). The EPMA data-based mole fraction of cheralite was 0.036 ± 0.012. Huttonite substitution was negligible. The USGS-44069 and TM monazites showed the same REE trends reported by Rubatto et al. (2014) (Fig. 2).

Oxygen isotopic composition

The bulk oxygen isotopic compositions of monazite RMs determined by laser fluorination are listed in Table 2.

Table 2 Oxygen isotopic compositions of the COM-1 and Hongcheon monazites, measured by gas-source mass spectrometry with laser fluorination

Sample	Date	Weight (mg)	Yield (%)	$\delta^{18}O_{VSMOW}$ (‰)	SD ($n=16$)
COM-1	8-September-2021	3.92	91.0	6.66	0.02
COM-1	4-May-2022	3.49	93.5	6.60	0.02
COM-1	4-May-2022	3.76	95.4	6.76	0.02
Average				6.67	0.08
Hongcheon-1	18-March-2019	2.29	90.8	6.60	0.02
Hongcheon-2	14-March-2019	2.54	90.9	6.13	0.01
Hongcheon-2	14-March-2019	3.29	92.0	6.03	0.02
Average				6.08	0.07

As noted in earlier studies (Breecker and Sharp, 2007; Rubatto et al., 2014; Didier et al., 2017), oxygen isotopic analysis of monazite by laser fluorination is challenging due to unstable yields of O_2 gas. Oxygen isotope data obtained by laser fluorination with F_2 (Rubatto et al., 2014; Didier et al., 2017) and BrF_5 gas (this study) clearly indicate that low yields of O_2 gas from samples result in relatively lower $\delta^{18}O$ values. Our data listed in Additional file 1: Table S1 show a distinct positive correlation between oxygen yields (42–96%) and measured $\delta^{18}O$ values (5.9–6.8 ‰) for the COM-1 monazite ($\delta^{18}O = 0.0151 \times$ yield (%) $+ 5.2806$, $R^2 = 0.80$).

O_2 gas yields lower than 90% cause mass-dependent fractionation in oxygen isotopes (up to 0.8‰ in $\delta^{18}O$) (Additional file 1: Table S1). Fluorination of monazite may produce POF_3 and unidentified $P-O-F_x$ gases in addition to O_2 gas (Breecker and Sharp, 2007; Jones et al., 1999). Kinetic fractionation of oxygen isotopes may occur in this process, which is followed by purification of O_2 gas and detection of isotopically fractionated O_2 gas by the mass spectrometer. Low $\delta^{18}O$ values with low O_2 gas yields likely indicate that light oxygen isotope (^{16}O) is preferentially fractionated into O_2 gas rather than into POF_3 and other $P-O-F_x$ gaseous species. Additionally, isotopic fractionation of O_2 gas may be related to the pressures in the bellows of the mass spectrometer (Yan et al., 2022). However, it should be noted that the change of $\delta^{18}O$ induced by this pressure-dependent fractionation is expected to be negligible ($< 0.1‰$) during routine oxygen isotope analyses of 6 to 8 samples. Regardless of the fractionation mechanism, it is clear that low O_2 gas yields of monazite during bulk-sample laser fluorination produce inaccurate data. Therefore only $\delta^{18}O$ values obtained with high O_2 yields ($>90\%$) were considered in this study.

Ayers et al. (2006) revealed no matrix effects for compositionally different monazites, but Breecker and Sharp (2007) reported that the IMF of oxygen isotopic measurements obtained using the same SIMS model (Cameca IMS1270) correlated with the monazite Th content. Rubatto et al. (2014) suggested that the IMF of SHRIMP oxygen measurements results from huttonite and cheralite substitutions in monazite. More recently, Didier et al. (2017) concluded that the IMF of Cameca IMS1280 measurements is a function of monazite [YREEPO$_4$], and less importantly, Th content. They showed that the IMF factor, defined as $\delta^{18}O_{laser\ fluorination}-\delta^{18}O_{SIMS}$, correlated positively with the YREE (and thus negatively with the Th) content, as also suggested by Breecker and Sharp (2007). Wu et al. (2020) proposed a power-law relationship between the IMF factor of Cameca IMS1280 oxygen isotope data and monazite Si content.

Our SIMS oxygen isotope data are presented with EPMA data in Additional file 3: Table S3. The three RMs introduced in this study had homogeneous oxygen isotopic compositions (SD $< 0.3‰$). The $\delta^{18}O$ difference between Hongcheon-1 and Hongcheon-2 was consistent within errors in the laser fluorination (0.52‰) and average SIMS results (0.54‰). Given their oxygen isotopic homogeneity and substantial differences in chemical composition, the COM-1 and Hongcheon monazites are useful materials with which to calibrate IMF-related SIMS effects. We calculated the IMF factor using laser fluorination results obtained in this study and the value reported for the USGS-44069 monazite (7.67‰; Rubatto et al., 2014). The IMF factor ($\delta^{18}O_{laser\ fluorination}-$average $\delta^{18}O_{SIMS}$) correlated inversely with the REE content ($R^2 = 0.99$), contrary to the conclusion reached by Didier et al. (2017), and weakly and nonlinearly with the Th and Ca contents (Fig. 3). Since the SIMS IMF is strongly affected by electron gun tuning and the configuration of secondary ion optics, the fractionation factor and its correlation trend with chemical compositions may differ among instruments. Indeed, Didier et al. (2017) and Wu et al. (2020) reported quite different IMF factors ($> 16‰$)

Kim *et al. Journal of Analytical Science and Technology*   (2022) 13:34

Page 7 of 8

Fig. 3 Secondary ion mass spectrometry $\delta^{18}O$ values plotted against inductively coupled plasma mass spectrometry-based total rare earth element and electron probe microanalyzer-based ThO_2 and CaO contents

from the same monazite standard materials, even though they utilized the same SIMS model (Cameca IMS1280) with similar analytical conditions. Our data defined a planar linear regression in a three-dimensional IMF versus Ca + Si 3D diagram (not shown), as Rubatto et al. (2014) suggested, but with a weak correlation coefficient ($R^2 = 0.7$). The TM monazite yielded an average corrected $\delta^{18}O_{VSMOW}$ value of $9.57 \pm 0.47‰$, obtained using the equation derived from our data ($\delta^{18}O_{corrected} = -0.301\,7 \times [\text{total REE, wt.\%}] + 18.085$; Fig. 3). This value awaits further verification.

Concluding remarks

In this study, we characterized chemical and oxygen isotopic compositions of the new monazite RMs COM-1 ($\delta^{18}O_{VSMOW} = 6.67 \pm 0.08‰$), Hongcheon-1 ($= 6.60 \pm 0.02‰$), and Hongcheon-2 ($= 6.08 \pm 0.07‰$). We conclude that the IMF of SIMS oxygen isotope measurement on monazite occurs differently from instrument to instrument, and IMF correction with well-established oxygen isotope standards is essential in every analytical session.

Abbreviations

BSE: Backscattered electron; EPMA: Electron probe microanalyzer; ICP-MS: Inductively coupled plasma mass spectrometry; IMF: Instrumental mass fractionation; KBSI: Korea Basic Science Institute; KOPRI: Korea Polar Research Institute; NIST: National Institute of Standards and Technology of the USA; REE: Rare earth element; RM: Reference material; SD: Standard deviation; SE:

Standard error; SHRIMP: Sensitive high-resolution ion microprobe; SIMS: Secondary ion mass spectrometry; SLAP: Standard light Antarctica precipitation; SMOW: Standard mean ocean water; SRM: Standard reference material; USGS: United States Geological Survey; VSMOW: Vienna Standard mean ocean water.

Supplementary Information

Author contributions

ACSC designed the research. ACSC, JK, and CP wrote the manuscript. JK, CP, KY, SL, SJK, and MJJ carried out the experiment and contributed to the interpretation of the results. All authors read and approved the final manuscript.

Kim *et al. Journal of Analytical Science and Technology*   (2022) 13:34

Page 8 of 8

Availability of data and materials
The data that support the findings of this study are available from the corresponding author upon reasonable request.

Declarations

Competing interests
The authors declare that they have no competing interests.

Author details
[1]Korea Basic Science Institute, Cheongju 28119, Republic of Korea. [2]Korea Polar Research Institute, Incheon 21990, Republic of Korea. [3]Graduate School of Analytical Science and Technology, Chungnam National University, Daejeon 34134, Republic of Korea.

References

Aleinikoff JN, Schenck WS, Plank MO, Srogi L, Fanning CM, Kamo SL, Bosbyshell H. Deciphering igneous and metamorphic events in high-grade rocks of the Wilmington Complex, Delaware: Morphology, cathodoluminescence and backscattered electron zoning, and SHRIMP U-Pb geochronology of zircon and monazite. Geol Soc Am Bull. 2006. https://doi.org/10.1130/B25659.1.

Ayers JC, Loflin M, Miller CF, Barton MD, Coath CD. In situ oxygen isotope analysis of monazite as a monitor of fluid infiltration during contact metamorphism: Birch Creek Pluton aureole, White Mountains, eastern California. Geology. 2006. https://doi.org/10.1130/G22185.1.

Baertschi P. Absolute ^{18}O Content of standard mean ocean water. Earth Planet Sci Lett. 1976. https://doi.org/10.1016/0012-821X(76)90115-1.

Breecker DO, Sharp ZD. A monazite oxygen isotope thermometer. Am Mineral. 2007. https://doi.org/10.2138/am.2007.2367.

Catlos EJ. Generalizations about monazite: Implications for geochronologic studies. Am Miner. 2013. https://doi.org/10.2138/am.2013.4336.

Cheong ACS, Jeong YJ, Lee S, Yi K, Jo HJ, Lee HS, Park C, Kim NK, Li XH, Kamo SL. LKZ-1: a new zircon working standard for the in situ determination of U-Pb age, O-Hf isotopes, and trace element composition. Minerals. 2019. https://doi.org/10.3390/min9050325.

Davidson JP, Morgan DJ, Charlier BLA, Harlou R, Hora JM. Microsampling and isotopic analysis of igneous rocks: Implications for the study of magmatic systems. Annu Rev Earth Planet Sci. 2007. https://doi.org/10.1146/annurev.earth.35.031306.140211.

Didier A, Putlitz B, Baumgartner LP, Bouvier AS, Vennemann TW. Evaluation of potential monazite reference materials for oxygen isotope analyses by SIMS and laser assisted fluorination. Chem Geol. 2017. https://doi.org/10.1016/j.chemgeo.2016.12.031.

Faure G, Mensing TM. Isotopes: principles and applications. 3rd ed. New York: John Wiley & Sons; 2005.

Foster G, Gibson HD, Parrish R, Horstwood M, Fraser J, Tindle A. Textural, chemical and isotopic insights into the nature and behaviour of metamorphic monazite. Chem Geol. 2002. https://doi.org/10.1016/S0009-2541(02)00156-0.

Hoefs J. Stable isotope geochemistry. 8th ed. Cham: Springer; 2018. https://doi.org/10.1007/978-3-319-78527-1.

Jochum KP, Weis U, Stoll B, Kuzmin D, Yang Q, Raczek I, Jacob DE, Stracke A, Birbaum K, Frick DA, Günther D, Enzweiler J. Determination of reference values for NIST SRM 610–617 glasses following ISO guidelines. Geostand Geoanal Res. 2011. https://doi.org/10.1111/j.1751-908X.2011.00120.x.

Jones AM, Iacumin P, Young ED. High-resolution δ^{18}O analysis of tooth enamel phosphate by isotope ratio monitoring gas chromatography mass spectrometry and ultraviolet laser fluorination. Chem Geol. 1999. https://doi.org/10.1016/S0009-2541(98)00162-4.

Kim N, Cheong ACS, Yi K, Jeong YJ, Koh SM. Post-collisional carbonatite-hosted rare earth element mineralization in the Hongcheon area, central Gyeonggi massif, Korea: Ion microprobe monazite U-Th-Pb geochronology and Nd-Sr isotope geochemistry. Ore Geol Rev. 2016. https://doi.org/10.1016/j.oregeorev.2016.05.016.

Kim NK, Kusakabe M, Park C, Lee JI, Nagao K, Enokido Y, Yamashita S, Park SY. An automated laser fluorination technique for high-precision analysis of three oxygen isotopes in silicates. Rapid Commun Mass Spectrom. 2019. https://doi.org/10.1002/rcm.8389.

Kim NK, Park C, Kusakabe M. Two-point normalization for reducing inter-laboratory discrepancies in δ^{17}O, δ^{18}O, and Δ'^{17}O of reference silicates. J Anal Sci Technol. 2020. https://doi.org/10.1186/s40543-020-00248-0.

Kim SJ, Lee TH, Yi K, Jeong YJ, Cheong CS. Characterization of new zircon and monazite working standards LKZ-1, BRZ-1, COM-1 and BRM-1. In: Paper presented at the 1st Japan-Korea SHRIMP meeting, Hiroshima University, Higashi-Hiroshima, pp. 14–16 September 2015.

McDonough WF, Sun SS. The composition of the Earth. Chem Geol. 1995. https://doi.org/10.1016/0009-2541(94)00140-4.

Meija J, Coplen TB, Berglund M, Brand WA, Bièvre PD, Gröning M, Holden NE, Irrgeher J, Loss RD, Walczyk T, Prohaska T. Isotopic compositions of the elements 2013 (IUPAC technical report). Pure Appl Chem. 2016. https://doi.org/10.1515/pac-2015-0503.

Möller A, Hensen BJ, Armstrong RA, Mezger K, Ballèvre M. U-Pb zircon and monazite age constraints on granulite-facies metamorphism and deformation in the Strangways Metamorphic Complex (central Australia). Contrib Mineral Petrol. 2003. https://doi.org/10.1007/s00410-003-0460-3.

Rubatto D, Putlitz B, Gauthiez-Putallaz L, Crépisson C, Buick IS, Zheng YF. Measurement of in-situ oxygen isotope ratios in monazite by SHRIMP ion microprobe: Standards, protocols and implications. Chem Geol. 2014. https://doi.org/10.1016/j.chemgeo.2014.04.029.

Sharp ZD. A laser-based microanalytical method for the in situ determination of oxygen isotope ratios of silicates and oxides. Geochim Cosmochim Acta. 1990. https://doi.org/10.1016/0016-7037(90)90160-M.

Sharp Z. Principles of stable isotope geochemistry. 2nd ed. New Mexico: The University of New Mexico; 2017. https://doi.org/10.25844/h9q1-0p82.

Valley JW. A cool early earth. Sci Am. 2005. https://doi.org/10.1038/scientificamerican1005-58.

Williams IS, Buick IS, Cartwright I. An extended episode of early Mesoproterozoic metamorphic fluid flow in the Reynolds range, central Australia. J Metamorph Geol. 1996. https://doi.org/10.1111/j.1525-1314.1996.00029.x.

Wu LG, Li QL, Liu Y, Tang GQ, Lu K, Ling XX, Li XH. Rapid and accurate SIMS microanalysis of monazite oxygen isotopes. J Anal Atom Spectrom. 2020. https://doi.org/10.1039/D0JA00069H.

Yan H, Peng Y, Bao H. Isotope fractionation during capillary leaking in an isotope ratio mass spectrometer. Rapid Commun Mass Spectrom. 2022. https://doi.org/10.1002/rcm.9290.

Publisher's Note

Springer Nature remains neutral with regard to jurisdictional claims in published maps and institutional affiliations.